46th AIAA Aerospace Sciences Meeting and Exhibit
7 - 10 January 2008, Reno, Nevada

AIAA 2008-503

Receptivity of A Hypersonic Flat-Plate Boundary Layer to Surface Roughness

Xiaowen Wang * **and Xiaolin Zhong** †
Mechanical and Aerospace Engineering Department
University of California, Los Angeles, California 90095

Abstract

The receptivity of a hypersonic flat-plate boundary layer to small surface roughness is investigated by series of numerical simulations. The main objectives of the current paper are to study the receptivity process of a Mach 5.92 flow over a flat plate to surface roughness and the effect of spanwise wave number on the receptivity. The free-stream flow conditions are the same as those of Maslov et al.'s leading-edge receptivity experiment [1]. Two-dimensional steady base flow is firstly achieved by solving compressible Navier-Stokes equations with a combination of a fifth-order shock-fitting method and a second-order TVD scheme. The accuracy of the numerical steady base flow is validated by comparisons with the theoretical self-similar boundary-layer solution and Maslov et al.'s experimental measurements. The three-dimensional base flow is directly extended from two-dimensional base flow due to the fact that the base flow over the flat plate is independent of spanwise coordinate. In receptivity simulations, small surface roughness, periodic in spanwise direction, is introduced on the flat plate. The subsequent responses of the hypersonic boundary layer are simulated by solving three-dimensional Navier-Stokes equations with a fifth-order shock-fitting method and a Fourier collocation method. Due to small height of roughness element, boundary conditions of temperature and velocities on the rough surface are transferred to original smooth surface by linear extrapolation. The effect of spanwise wave number on the receptivity is studied by considering six cases of receptivity simulations. The numerical results show that counter rotating streamwise vortices and transient growth are induced by surface roughness. The spanwise wave number has a strong effect on the excitation of transient growth. For the six cases considered in current study, surface roughness with the spanwise wave number being 0.0101 has the strongest excitation of transient growth.

1 Introduction

The laminar-turbulent transition of the boundary-layer flows has a significant effect on drag calculation and aerothermal design of hypersonic vehicles. In order to predict and control boundary-layer transition, extensive studies have been carried out to reveal transition mechanisms [2, 3, 4, 5, 1, 6]. It is recognized that the transition process of a boundary-layer flow strongly depends on the amplitude level of environmental perturbations [7, 8, 9], which is schematically shown in Fig. 1. In an environment of small amplitude perturbations, transition of the boundary-layer flow over a smooth surface generally consists of three step: 1) Receptivity process during which small amplitude environmental disturbances enter the boundary layer and excite boundary-layer wave modes; 2) Linear development or growth of unstable boundary-layer wave modes which can be predicted by solving the eigen-problem of the homogeneous linearized stability equations; 3) Boundary-layer transition caused by non-linear breakdown and three-dimensional effects when the unstable wave modes reach certain amplitudes. For high amplitude perturbations, laminar boundary-layer flow can breakdown to turbulence right after the receptivity process due to the strong initial excitations of boundary-layer wave modes. On non-smooth surface with roughness elements, the strong transient growth of boundary-layer wave modes may directly lead to transition [7, 8, 9]. All these transitions relating to high amplitude perturbations and transient growth are called bypass transition.

The study of receptivity process is of critical importance to the predict of transition because it provides initial

*Postdoctoral Researcher,Mechanical and Aerospace Engineering Department, AIAA Member.
†Professor, Mechanical and Aerospace Engineering Department, AIAA Associate Fellow.

conditions of amplitude, frequency, and phase angle for boundary-layer wave modes [10]. Recently, theoretical, experimental, and numerical simulation studies on the receptivity of two and three-dimensional boundary layers have been carried out by many researchers [1, 11, 12, 13, 14].

Mack [3] used compressible LST to calculate the amplitude ratio of constant-frequency disturbances for insulated and cooled-wall flat-plate supersonic boundary layers. He found that the ratio of transition Reynolds numbers calculated from LST for insulated and cooled-wall cases increased much faster than the experimental results. LST alone was insufficient to determine the transition Reynolds number, and it was necessary to consider the properties of the environmental disturbances and the initial excitations of boundary-layer wave modes. Balakumar et al. [15] investigated the evolution of small amplitude travelling disturbances in a rotating disk flow, where the disturbances were generated by perturbing the steady rotational speed of the disk and introducing roughness elements on disk surface. They found that only eigensolutions at frequencies larger than 4.58 times of the steady disk rotational frequency grew algebraically in radial direction. Their results of receptivity coefficient computations showed that these eigensolutions were excited the most when the width of roughness elements in radial direction was about the radial location of the roughness. By solving the nonlinear parabolized stability equations (PSE), Bertolotti [16] studied the amplification of vortices over a plate generated by surface roughness, blowing-suction, or both. The results showed that the growth of vorticity could be much larger with the presence of both wall inhomogeneities. Choudhari [17] studied the roughness-induced generation of stationary and nonstationary vortices in three-dimensional boundary layers over a sweep wing, where nonstationary vortices were induced with the presence of free-stream acoustic disturbances. The effects of acoustic-wave orientation and different types of roughness geometries were considered. It was found that maximum receptivity occurred when the velocity fluctuation of acoustic disturbance was aligned with the wave-number vector of nonstationary vortex mode. Hanifi et al. [18] investigated transient growth phenomena of boundary-layer flows with a series of Mach numbers from 0.1 to 4.5 using spectral collocation method. They found that maximum transient growth increased with Mach number and could be scaled with the square of local Reynolds number. Andersson et al. [19] numerically calculated the maximum transient growth for steady disturbances and concluded that optimal disturbances consisted of streamwise vortices. They also found that maximum transient growth scaled linearly with the distance from the leading edge. Herbert [20] considered the stability and transition of 3D boundary layers varying both in streamwise and spanwise directions by extending the PSE to 3D boundary layers. The analysis of cross-flow dominated flow showed that the vector of growth rates (α_i, β_i) cannot be solely determined from the local flow characteristics and careful attention must be paid to initial conditions. Reshotko [21] investigated the spatial transient growth by examining examples including Poiseuille flow, hypersonic blunt body paradox and distributed roughness effects. It was demonstrated that bypass transition could be explained by transient growth thoery. Fedorov and Khokhlov [11] studied the receptivity of hypersonic boundary layers over a flat plate to wall disturbances using a combination of asymptotic method and numerical simulation. They investigated the receptivity process to different wall disturbances, i.e., wall vibrations, periodic blowing-suctions, and temperature disturbances. It was found that strong excitations occurred in local regions where forcing disturbances were resonant with boundary-layer wave modes. For boundary layers on cool surfaces, the resonance point approached the branch point of discrete spectrum, and the receptivity coefficient tended to infinity. By using asymptotic method, this singularity was successfully resolved and receptivity coefficient near the brach point was achieved. Their numerical results indicated extremely high receptivity near the Branch I neutral point of mode S. They also found that hypersonic boundary layers were more sensitive to blowing-suction disturbances than to wall vibrations and temperature disturbances. Forgoston and Tumin [22] studied a three-dimensional wave packet generated by a local temperature slot in a hypersonic boundary layer. They showed that the solution to this initial-value problem could be expanded in a biorthogonal eigenfunction system as a sum of discrete and continuous modes. The inverse Fourier transforms for mode F and mode S were computed and agreed well with the asymptotic approximation of the Fourier integral for sufficiently large time. Recently, Tumin [12] solved the receptivity problem of compressible boundary layers to three-dimensional wall perturbations by using biorthogonal eigenfunction system. In case of receptivity to roughness elements, a small height hump was considered. The results showed that there were counter rotating streamwise vortices, streaks at both sides of the hump, and a wake region downstream from the hump. In supersonic boundary layers, there existed large amplitude perturbations near the Mach waves generated by roughness elements.

Due to the difficulties in carrying out supersonic and hypersonic receptivity experiments, very few experimental studies have been reported. Kendall [4] experimentally studied the origin and growth of natural fluctuations in zero pressure-gradient boundary layers of several Mach numbers ranging from 1.6 to 8.5. Substantial growths of flow fluctuations were observed within the laminar boundary layer in the early region where the boundary

layer was predicted to be linearly stable. These fluctuations were found to be related to the acoustic noise for hypersonic flows. The growth rates of these fluctuations in the region downstream of the initial growth were in a reasonable agreement with the LST results of Mack [3]. Maslov and Semenov [23] experimentally investigated the receptivity of a supersonic boundary layer to artificial acoustic waves by utilizing two parallel flat plates. The acoustic waves generated by an electric discharge system on the lower plate radiated into the external flow and penetrated into the boundary layer of the upper plate as free-stream acoustic disturbances. It was found that the acoustic disturbances were converted into boundary-layer wave modes most efficiently at the leading edge, in the neighborhood of the acoustic branch of the neutral curve, and in the vicinity of lower branch of the neutral curve. A similar experiment was carried out at a Mach 5.92 flow by Maslov et al. [1] to study the leading edge receptivity of the hypersonic boundary layer. It was observed that Tollmien-Schlichting waves were generated by the acoustic waves impinging on the leading edge. They also found that the receptivity coefficients depended on wave inclination angles. Gaster et al. [24] measured the velocity disturbance in a flat plate boundary layer induced by a three-dimensional shallow bump oscillating at a frequency of 2 Hz. It was observed that the intensity of velocity disturbance reached its maximum near $\eta = 2$ at a location about 100 boundary-layer thickness downstream of the bump. They also noticed a small secondary peak in the spanwise spectrum near the bump. Bakchinov et al. [25] studied the stability of an incompressible boundary layer over a flat plate. The experiments were carried out in a low speed wind tunnel. Inside the boundary layer, roughness elements were arranged in spanwise direction to generate stationary streamvise vortices. Small amplitude travelling waves were introduced to the boundary layer on top of the steady vortices. According to their results, the maximum amplification of wave amplitude was found at a wall-normal position where the mean streamwise velocity was equal to wave phase velocity. Vetlutskii et al. [26] experimentally measured density profiles of a hypersonic nitrogen flow on a flat plate using the method of electron-beam fluorescence. On the other hand, the model of a viscous shock layer was used to calculate the hypersonic flow. They found that the experimental measurements and numerical calculations of density profiles had a good agreement. In order to evaluate the optimal-disturbance theories, White [27] investigated the transient growth of a flat plate boundary layer to controlled stationary disturbances generated by using spanwise roughness array. The results showed quantitative differences between experimental measurements and theoretical predictions, which did indicate that realistic stationary disturbances could exhibit significant nonoptimal behavior. White and Ergin [28] further studied the receptivity and transient growth of a Blasius boundary layer to roughness-induced disturbances, where the initial disturbances were generated by a spanwise array of roughness elements. In experiments, detailed information on the disturbances and the transient growth was measured using hotwire instruments. The results indicated that energy associated with the roughness-induced disturbances scaled with the roughness-based Reynolds number. Fransson et al. [29] experimentally and theoretically investigated the transient growth of stationary streamwise streaks in a flat plate boundary layer. The stable laminar streaks was periodic in spanwise direction and was generated by a spanwise periodic array of small cylindrical roughness elements. The results showed that the maximum transient growth was mainly determined by the height of roughness elements. Recently, White et al. [30] investigated the effects of the amplitude and diameter of cylindrical roughness elements on transient growth features. Their experimental results showed that energy of stationary disturbances varied as Re_k^2, the square of roughness-based Reynolds number, and the qualitative nature of transient growth strongly depended on the roughness diameter.

Recently there are many numerical simulation studies in supersonic and hypersonic boundary-layer receptivity. Kawamura et al. [31] analyzed incompressible high-Reynolds-number flows around a cylinder with surface roughness by integrating Navier-Stokes equations using finite difference method. In their computations, the height of roughness elements was half percent of the cylinder diameter. They observed a sharp drag-coefficient reduction near the Reynolds number of 20000. Joslin and Grosch [32] computed the disturbance velocity field downstream of a shallow bump in a laminar boundary layer by direct numerical simulation of incompressible Navier-Stokes equations. The flow conditions in their simulation was the same as the experimental parameters of Gaster et al. [24]. According to the simulation results, modal growth and decay trends of velocity disturbance were consistent with Gaster et al.'s experimental measurements. Bottaro and Zebib [33] numerically investigated the formation and growth of spatial Görtler vortices induced by wall roughness. In all naturally developing cases, the average spanwise wavelengths of vortices were close to those of optimal disturbances predicted by LST. Stemmer et al. [34] studied the laminar-turbulent transition mechanisms of a flat plate boundary layer to a harmonic point source disturbances by numerical simulations based on the Navier-Stokes equations for three-dimensional incompressible flow. The results for early stages agree very well with LST results and with in-flight experiments. Collis and Lele [35] numerically investigated the formation of stationary crossflow vortices in a three-dimensional boundary layer due to surface roughness

near the leading edge of a swept wing. The results showed that convex surface curvature enhanced receptivity while non-parallel effects strongly reduced the initial amplitude of stationary crossflow vortices. Malik et al. [5] investigated the responses of a Mach 8 flow over a sharp wedge of a half-angle of 5.3° to three types of external forcing: a planar free-stream acoustic wave, a narrow acoustic beam enforced on the bow shock near the leading edge, and a blowing-suction slot on the wedge surface. They concluded that these three types of forcing eventually result in the same type of instability waves in the boundary layer. Zhong [36] studied the acoustic receptivity of a hypersonic flow over a parabola by solving full Navier-Stokes equations. It was concluded that the generations of boundary-layer wave modes were mainly owing to the interaction of the boundary layer with the transmitted acoustic waves instead of entropy and vorticity waves. In a series of papers, Ma and Zhong [13, 14, 6] studied the receptivity of a supersonic boundary layer to various free-stream disturbances by a combination of numerical simulation and linear stability theory. It was found that, in addition to the conventional first and second Mack modes, there existed a family of stable modes which played an important role in the excitation of unstable modes. Dong and Zhong [37] carried out parametric simulations of receptivity to free-stream disturbances of a Mach 15 flow over 3D blunt leading edges by using high-order shock-fitting finite difference method on parallel clusters. The results showed that the magnitude of transient growth inside the boundary layer increased by introducing random roughness strips on the wall. Egorov et al. [38] simulated unsteady two-dimensional flows relevant to receptivity of supersonic and hypersonic boundary layers by using a TVD scheme. For small forcing amplitudes, the second-mode growth rates obtained by numerical simulation agreed well with those predicted by LST including the non-parallel effects. The results of their simulations showed a non-linear saturation of fundamental harmonic and rapid growth of higher harmonics. Choudhari and Fischer [39, 40] examined the roughness-induced transient growth in a laminar boundary layer due to a spanwise periodic array of circular disks at the surface. The effects of roughness height, size, and shape on the transient growth were also explored. Their numerical simulation results indicated that energy levels of the dominant stationary disturbances were consistent with the Re_k^2 scaling of White et al. [30]. Spontaneous vortex shedding behind the roughness array was identified for sufficiently large roughness heights. Ma and Zhong [41] studied the receptivity of the same hypersonic boundary layer as in Malik et al.'s [5] investigation to various free-stream disturbances, i.e., fast and slow acoustic waves, vorticity waves, and entropy waves, by solving the two-dimensional compressible Navier-Stokes equations. They found that the stable modes in the boundary layer played a very important role in the receptivity process. Wang and Zhong [42] investigated the receptivity of the same flow over the sharp wedge to periodic blowing-suction disturbances introduced in a narrow region on the wall. The effects of frequency, location, and length of the blowing-suction actuator on the receptivity process were also investigated based on series of numerical simulations. The numerical results showed that mode F, mode S, and acoustic modes were excited by the blowing-suction disturbances. Far downstream of the forcing region, mode S became the dominant mode in the boundary layer. All cases of numerical simulations consistently showed that the synchronization point of mode F and mode S played an important role in the excitation of mode S by wall blowing-suction. Mode S was strongly excited when the blowing-suction actuator was located upstream of the synchronization point. On the other hand, when the blowing-suction actuator was downstream of the synchronization point, there was a very weak excitation of mode S, despite the fact that the blowing-suction actuator was still within the unstable region of mode S. A concurrent theoretical study had been carried out by Tumim, Wang, and Zhong [12] to compare the theoretical and numerical results of receptivity coefficients and to analyze the receptivity characteristics. The perturbation flow field downstream of the blowing-suction actuator was decomposed into boundary-layer wave modes with the help of the biorthogonal eigenfunction system. It was found that there was a good agreement between normal-mode amplitudes calculated with the help of the theoretical receptivity model and those obtained by projecting the numerical results onto the normal modes. Egorov et al. [43] studied the stability and receptivity of a Mach 6 flow on a flat plate with a porous coating by numerically solving the two-dimensional Navier-Stokes equations. Their numerical results were in good agreement with the theoretical analysis based on LST. According to their results, the concept of the stabilization of the supersonic boundary layer by a porous coating was confirmed. Zhong and Ma [44] numerically studied the receptivity to weak free-stream fast acoustic waves of a Mach 7.99 axisymmetric flow over a 7° half-angle blunt cone. They found that no Mack modes were excited by free-stream fast acoustic waves in the early region along the cone surface. The delay of the second-mode excitation was owing to the fact that the hypersonic boundary-layer receptivity was governed by a two-step resonant interaction process.

In this paper, the receptivity of a hypersonic flat-plate boundary layer to small surface roughness is studied by series of numerical simulations. The objectives of the current paper are to study the receptivity process of the hypersonic boundary layer to surface roughness, and to investigate the effect of spanwise wave number on

the receptivity. The free-stream flow conditions are the same as those of Maslov et al.s leading-edge receptivity experiments. Two-dimensional steady base flow is firstly achieved by solving compressible Navier-Stokes equations with a combination of a fifth-order shock-fitting method and a second-order TVD scheme. The accuracy of the numerical steady base flow is validated by comparisons with the theoretical self-similar boundary-layer solution and Maslov et als experimental measurements. The three-dimensional base flow is directly extended from two-dimensional base flow due to the fact that the base flow over the flat plate is independent of spanwise coordinate. In receptivity simulations, small surface roughness periodic in spanwise direction is introduced on the flat plate. The subsequent responses of the hypersonic boundary layer are simulated by solving three-dimensional Navier-Stokes equations with a fifth-order shock-fitting method and a Fourier collocation method. Due to small height of roughness element, boundary conditions on the rough surface is transferred to the smooth flat flate by linear extrapolation, which is validated based on numerical simulations of different height surface roughness. The effect of spanwise wave number on the receptivity is studied by considering six cases of receptivity simulations.

2 Governing Equations and Numerical Methods

In the current numerical studies, a Mach 5.92 flow over a flat plate as shown in Fig. 2 is considered. The flow is assumed to be thermally and calorically perfect. The governing equations for the simulation are the full Navier-Stokes equations in the conservative form, i.e.,

$$\frac{\partial \vec{U}^*}{\partial t^*} + \frac{\partial}{\partial x_1^*}(\vec{F}_{1i}^* + \vec{F}_{1v}^*) + \frac{\partial}{\partial x_2^*}(\vec{F}_{2i}^* + \vec{F}_{2v}^*) + \frac{\partial}{\partial x_3^*}(\vec{F}_{3i}^* + \vec{F}_{3v}^*) = 0 \tag{1}$$

where the superscript "$*$" represents the dimensional variables. $\vec{U}^*$ is a vector containing the conservative variables of mass, momentum, and energy, i.e.,

$$\vec{U}^* = \{\rho^*, \rho^* u_1^*, \rho^* u_2^*, \rho^* u_3^*, e^*\} \tag{2}$$

The flux vector in Eq. (1) is divided into its inviscid and viscous components, because the two components are discretized with different schemes. The components, $\vec{F}_{1i}^*$, $\vec{F}_{2i}^*$, $\vec{F}_{3i}^*$, are inviscid flux vectors whereas $\vec{F}_{1v}^*$, $\vec{F}_{2v}^*$, and $\vec{F}_{3v}^*$ are viscous flux vectors. The flux vectors can be expressed as

$$\vec{F}_{ji}^* = \begin{bmatrix} \rho^* u_j^* \\ \rho^* u_1^* u_j^* + p^* \delta_{1j} \\ \rho^* u_2^* u_j^* + p^* \delta_{2j} \\ \rho^* u_3^* u_j^* + p^* \delta_{3j} \\ u_j^*(e^* + p^*) \end{bmatrix}, \quad \vec{F}_{jv}^* = \begin{bmatrix} 0 \\ -\tau_{1j}^* \\ -\tau_{2j}^* \\ -\tau_{3j}^* \\ -\tau_{1j}^* u_1^* - \tau_{2j}^* u_2^* - \tau_{3j}^* u_3^* + k^* \frac{\partial T^*}{\partial x_j^*} \end{bmatrix} \tag{3}$$

with $j \in \{1, 2, 3\}$. In Eq. (3), δ_{ij} $(i = 1, 2, 3)$ is the Kronecker Delta function. In the perfect gas assumption, pressure and energy are given by

$$p^* = \rho^* R^* T^* \tag{4}$$

$$e^* = \rho^* c_v^* T^* + \frac{\rho^*}{2}(u_1^{*2} + u_2^{*2} + u_3^{*2}) \tag{5}$$

where c_v^* is the specific heat at constant volume. For compressible Newtonian flow, the viscous stress tensor can be written as:

$$\tau_{ij}^* = \mu^* \left(\frac{\partial u_i^*}{\partial x_j^*} + \frac{\partial u_j^*}{\partial x_i^*} \right) - \frac{2}{3}\mu^* \left(\frac{\partial u_1^*}{\partial x_1^*} + \frac{\partial u_2^*}{\partial x_2^*} + \frac{\partial u_3^*}{\partial x_3^*} \right) \delta_{ij} \tag{6}$$

with $i, j \in \{1, 2, 3\}$. In the simulation, the viscosity coefficient, μ^*, and the heat conductivity coefficient, k^*, are calculated using the Sutherland's law together with a constant Prandtl number, Pr. They are both functions of temperature only.

$$\mu^* = \mu_r^* \left(\frac{T^*}{T_r^*} \right)^{3/2} \frac{T_r^* + T_s^*}{T^* + T_s^*} \tag{7}$$

$$k^* = \frac{\mu^* c_p^*}{Pr} \tag{8}$$

where $\mu_r^* = 1.7894 \times 10^{-5}$ Ns/m^2, $T_r^* = 288.0$ K, $T_s^* = 110.33$ K, and c_p^* is the specific heat at constant pressure. In this paper, the dimensional flow variables are non-dimensionalized by free-stream parameters. Specifically, density ρ^*, temperature T^*, velocities u_1^*, u_2^*, u_3^*, and pressure p^* are non-dimensionalized by ρ_∞^*, T_∞^*, u_∞^*, and $\rho_\infty^* u_\infty^{*2}$. Furthermore, x_1^* and x_3^* is non-dimensionalized by unit length in meter, whereas x_2^* is non-dimensionalized by Blasius boundary-layer thickness, $\sqrt{\mu_\infty^* x_1^* / \rho_\infty^* u_\infty^*}$. Referring to the coordinate system shown in Fig. 2, x_1^*, x_2^*, and x_3^* are x^*, y^*, and z^*, respectively. The three variables, u_1^*, u_2^*, and u_3^*, are velocities in streamwise, wall-normal, and spanwise directions.

The high-order shock-fitting finite difference method of Zhong [45] is used to solve the governing equations in a domain bounded by the bow shock and the flat plate. In orther words, the bow shock is treated as a boundary of the computational domain. The Rankine-Hugoniot relation across the shock and a characteristic compatibility relation coming from downstream flow field are combined to solve the flow variables behind the shock. The shock-fitting method makes it possible for the Navier-Stokes equations to be spatially discretized by high-order finite difference methods. Specifically, a fifth-order upwind scheme is used to discretize the inviscid flux derivatives. Meanwhile, a sixth-order central scheme is used to discretize the viscous flux derivatives. For three-dimensional simulations, flux derivatives of $\vec{F}_{3i}^*$ and $\vec{F}_{3v}^*$ in spanwise direction are calculated by Fourier collocation method to achieve high accuracy. By using the shock-fitting method, the interaction between the bow shock and perturbations induced by wall disturbances is solved as a part of solutions with the position and velocity of the shock front being taken as dependent flow variables. A three-stage semi-implicit Runge Kutta method of Zhong et al. [46] is used for temporal integration. In the leading edge region, there exists a singular point at the tip of the flat plate, which introduces numerical instability if the fifth-order shock-fitting method is used to simulate the flow. Therefore, the computational domain for the shock-fitting simulation starts from a very short distance downstream of the leading edge. A second-order TVD scheme of Zhong and Lee [47] is used to simulate the steady base flow in a small region including the leading edge to supply inlet conditions for the shock-fitting simulation. For receptivity simulations, three-dimensional small-scale roughness elements are introduced in a downstream region where the shock-fitting method is used.

The same numerical method has been used by Ma and Zhong in their receptivity studies of supersonic and hypersonic boundary layers over a flat plate and a sharp wedge to various free-stream disturbances [13, 14, 6, 41]. The good agreement between numerical and LST results indicates that the high-order shock-fitting finite difference method is accurate to simulate the receptivity problems of high-speed boundary-layer flows. The numerical method has also been validated in the theoretical study and comparison with numerical simulation of Tumin, Wang, and Zhong [48]. The numerical perturbation field downstream of the blowing-suction actuator is decomposed into boundary-layer wave modes with the help of the biorthogonal eigenfunction system. The filtered-out amplitudes of mode S and mode F agree well with the theoretical solutions of linear receptivity problem. The Fourier collocation method has been tested by Zhong [49] to study the receptivity of a Mach 6 flow over a flared cone to free-stream disturbances. The numerical results are compared with published experiment results. It is found that the steady base flow solutions agree very well with the experiment results. The wave numbers and growth rates of numerical solutions are reasonably similar to the LST results.

3 Flow Conditions and Linear Boundary Condition Transfer

Free-stream flow conditions of the currently studied flow are the same as those of Maslov et al.'s experiment [1], i.e.,

$$M_\infty = 5.92\,, \qquad T_\infty^* = 48.69\text{K}\,,$$
$$p_\infty^* = 742.76\text{Pa}\,, \qquad Pr = 0.72\,,$$
$$Re_\infty^* = 13 \times 10^6/\text{m}$$

The dimensional streamwise coordinate, x^* as shown in Fig. 2, can be converted to the local Reynolds number by

$$Re_x = Re_\infty^*\, x^* \tag{9}$$

where Re_∞^* is the unit Reynolds number defined as

$$Re_\infty^* = \rho_\infty^* u_\infty^* / \mu_\infty^* \tag{10}$$

In LST studies of boundary-layer flows, the Reynolds number based on Blasius boundary-layer thickness, L^*, is generally used. They are expressed as

$$R = \frac{\rho_\infty^* u_\infty^* L^*}{\mu_\infty^*}, \quad L^* = \sqrt{\frac{\mu_\infty^* x^*}{\rho_\infty^* u_\infty^*}} \tag{11}$$

Hence, the relation between R and local Reynolds number Re_x is given by

$$R = \sqrt{Re_x} \tag{12}$$

For the simulation of base flow, the wall is adiabatic, and the physical boundary condition of velocity on the flat plate is the non-slip condition. When small surface roughness is introduced on the flat plate, boundary conditions of temperature and velocities on the rough surface are transferred to original smooth surface by linear extrapolation due to small height of roughness element. Figure 3 schematically shows the linear boundary condition transfer of streamwise velocity, where the blue arrows stand for the streamwise velocity boundary conditions for points A and B on original smooth surface. Therefore, the computational domain and grid structure of receptivity simulation are the same as those of base flow simulation. In smooth region, adiabatic thermal condition and non-slip condition are used. Inlet conditions are specified, while high-order extrapolation is used for outlet conditions because the flow is hypersonic at the exit boundary except a small region near the flat plate.

Due to the existence of small roughness, the wall surface changes from $y^* = 0$ to $y^* = \epsilon\hbar^*(x^*, z^*)$, where $y^* = 0$ stands for original smooth surface. The function, $\hbar^*(x^*, z^*)$, represents the profile of roughness elements. The parameter, ϵ, is used to adjust the height. The physical non-slip conditions of velocity on the rough surface are

$$\begin{cases} u^*(x^*, \epsilon\hbar^*(x^*, z^*), z^*) = 0 \\ v^*(x^*, \epsilon\hbar^*(x^*, z^*), z^*) = 0 \\ w^*(x^*, \epsilon\hbar^*(x^*, z^*), z^*) = 0 \end{cases} \tag{13}$$

Under the assumption of small-height roughness elements, boundary conditions on the rough wall can be transferred to original smooth surface by linear extrapolation, i.e.,

$$\begin{cases} u^*(x^*, 0, z^*) = -\epsilon\hbar^*(x^*, z^*)\frac{\partial u^*}{\partial y^*} \mid_{y^*=0} \\ v^*(x^*, 0, z^*) = -\epsilon\hbar^*(x^*, z^*)\frac{\partial v^*}{\partial y^*} \mid_{y^*=0} \\ w^*(x^*, 0, z^*) = -\epsilon\hbar^*(x^*, z^*)\frac{\partial w^*}{\partial y^*} \mid_{y^*=0} \end{cases} \tag{14}$$

From our previous study [50], it was found that the roughness element on adiabatic flat plate was more efficient in the excitations of streamwise vortices and transient growth. Therefore, the adiabatic temperature condition is used on rough surface, which is expressed as

$$\frac{\partial T^*(x^*, \epsilon\hbar^*(x^*, z^*), z^*)}{\partial y^*} = 0 \tag{15}$$

Similarly, the temperature condition can be transferred to original smooth surface as follows:

$$\frac{\partial T^*(x^*, 0, z^*)}{\partial y^*} = -\epsilon\hbar^*(x^*, z^*)\frac{\partial^2 T^*}{\partial y^{*2}} \mid_{y^*=0} \tag{16}$$

In Eqs. (14) and (16), all derivatives on the right-hand-side of equations are calculated from the base flow.

For the roughness elements considered in current paper, the function of $\hbar^*(x^*, z^*)$ is defined as

$$\hbar^*(x^*, z^*) = \hbar^*(l)\cos(\beta^* z^*) \tag{17}$$

where β^* is the spanwise wave number. The function $\hbar^*(l)$ and the variable l are defined as

$$\hbar^*(l) = (20.25l_4^5 - 35.4375l_4^4 + 15.1875l_4^2)/2.45688 \tag{18}$$

$$l = 0.620287 \times \begin{cases} 2(x^* - x_i^*)/(x_e^* - x_i^*) & \text{if} \quad x^* \le 4.28125\text{mm} \\ 2(x_e^* - x^*)/(x_e^* - x_i^*) & \text{if} \quad x^* \ge 4.28125\text{mm} \end{cases} \tag{19}$$

The coordinates of the leading and trailing edges of the roughness elements in streamwise direction, x_i^* and x_e^*, are equal to 3.3125 mm and 5.25 mm, corresponding to $R = 216.31$ and $R = 272.32$, respectively. The constant, 2.45688, is the value of $\hbar^*(l)$ at $l = 0.620287$, which is used to normalize the profile function. Figure 4 shows the profile function $\hbar^*(l)$ and the variable l of the roughness element in streamwise direction. It is clearly shown that both $\hbar^*(l)$ and l are symmetric within the roughness region of 3.3125 mm $\leq x^* \leq$ 5.25 mm. And the height of surface roughness reaches its maximum at the center.

4 Results and Discussions

4.1 Steady base flow

Two-dimensional steady base flow over the flat plate is firstly simulated by solving the two-dimensional compressible Navier-Stokes equations with a combination of a fifth-order shock-fitting finite difference method and a second-order TVD scheme. The three-dimensional base flow is directly extended from two-dimensional base flow due to the fact that the base flow on the flat plate is independent of spanwise coordinate. Receptivity simulations are carried out by imposing wall disturbances to three-dimensional base flow. Since we already have two-dimensional steady base flow, such treatment is much more efficient than directly solving full Navier-Stokes equations with uniform initial conditions.

In the leading edge region, there exists a singular point at the tip of the flat plate, which will introduce numerical instability if the fifth-order shock-fitting method is used to simulate the flow. A second-order TVD scheme used by Zhong and Lee [47] is applied to simulate the steady base flow in a small region including the leading edge. The computational domain for the fifth-order shock-fitting method starts at $x^* = 0.0025$ m and ends at $x^* = 0.879$ m, corresponding to $R = 180.28$ and $R = 3380.38$, respectively. In actual shock-fitting simulations, the computational domain is divided into 19 zones with a total of 3746 grid points in streamwise direction. The number of grid points in wall-normal direction is 121 before the position of $x^* = 0.309$ m and 176 after that position. Forty-one points are used in the overlap region between two neighboring zones, which is proved to be sufficient to make the solution accurate and smooth within the whole domain. An exponential stretching function is used in the wall-normal direction to cluster more points inside the boundary layer. On the other hand, the grid points are uniformly distributed in streamwise direction. The spatial convergence of the results based on this grid structure has been evaluated by grid refinement studies to ensure the grid independence of the fifth-order shock-fitting simulations.

For shock-fitting simulation in the first zone, the inlet conditions are obtained from the results of the second-order TVD shock-capturing scheme which is used to simulate the steady base flow in a small region including the leading edge. For other zones, inlet conditions are interpolated from the results of the previous zone. The computational domain for the second-order TVD scheme starts at $x^* = -0.0005$ m and ends at $x^* = 0.0035$ m. In order to validate the combination of fifth-order shock-fitting method and second-order TVD scheme, Figs. 5 and 6 plot density and wall-normal velocity contours near the leading edge of the steady base flow obtained by the combination of second-order TVD scheme and fifth-order shock-fitting method. The flow field including the leading edge is simulated by the TVD scheme, while the flow field after $x^* = 0.0025$ m is simulated by the shock-fitting method. These figures show that density and wall-normal velocity contours calculated by the two methods have a good agreement near the upstream edge of the overlapped region, which indicates that the TVD solutions are accurate enough to be used as inlet conditions for the fifth-order shock-fitting simulation in the first zone. The small discrepancies of the contours near the bow shock are caused by viscous effect. Due to viscosity, the bow shock has a finite thickness for TVD simulation, while it is assumed to be infinitely thin for the shock-fitting simulation. The combination of fifth-order shock-fitting method and second-order TVD scheme has also been validated in cases of supersonic and hypersonic steady base flows by Ma & Zhong [51] and Wang & Zhong [42].

Figure 7 shows pressure contours of the steady base flow simulated by the fifth-order shock-fitting finite difference method. The upper boundary of the flow field represents the bow shock induced by the displacement thickness of the boundary layer. The lower boundary is the surface of the flat plate. A part of the pressure field from $x^* = 0.03$ m to $x^* = 0.08$ m is amplified to show clearly the pressure contours within the boundary layer. It is noticed that pressure is approximately a constant across the boundary layer and along the Mach lines, which is consistent with the theories of boundary-layer flow and inviscid supersonic aerodynamics. At a fixed location (constant x^*), pressure behind the shock is higher than that on the flat plate due to the existence of the bow shock. More results of the two-dimensional steady base flow were discussed in our previous papers [52, 50].

In order to validate the accuracy of numerical simulation, the steady base flow simulated by the fifth-order shock-fitting method is compared with the theoretical self-similar boundary-layer solution and Maslov et al.'s experimental

measurements. Figure 8 shows the distributions of dimensionless streamwise velocity across the boundary layer at three different locations. It shows that the thickness of the boundary layer increases with the location shifting downstream. At $x^* = 96$ mm, 121 mm, and 138 mm, the thicknesses of the boundary layer are approximately equal to 18.4 mm, 20.4 mm, and 22 mm, which has a good agreement with Maslov et al.'s experimental results of 18 mm, 20 mm, and 22 mm, respectively.

Figures 9 and 10 compare normalized Mach number M/M_∞ and dimensionless streamwise velocity u^*/u^*_∞ distributions across the boundary layer at three different locations of $x^* = 96$ mm, 121 mm, and 138 mm. In these figures, η is defined as $\eta = y^*/L^*$. The solid lines represent distributions of M/M_∞ and u^*/u^*_∞ obtained by solving the compressible boundary-layer equations. Due to the fact that the solution of boundary-layer equations is self-similar, the distributions of M/M_∞ and u^*/u^*_∞ at different locations are exactly the same for the boundary-layer solution. The unfilled symbols represent experimental results of Maslov et al., whereas the other three lines stand for numerical results simulated by the shock-fitting method. The good agreement between the simulation results indicate that an approximate gradientless flow is obtained over the flat plate, which is evaluated in Maslov et al.'s paper by comparing the experimental results. Figures 9 and 10 show that the numerical results agree well with the experimental results and the boundary-layer solution near the plate. However, in the region of $\eta > 5$, the numerical results have a better agreement with the experimental results. The difference between the numerical results and the boundary-layer solution is mainly caused by viscous-inviscid interaction, because the effect of the bow shock is neglected in the calculation of the compressible boundary-layer equations. The analysis of Figs. 8, 9, and 10 indicate that the fifth-order shock-fitting method is accurate to simulate the hypersonic flow considered in the current study.

4.2 Receptivity to small surface roughness

In compressible boundary layer, Tumin and Reshotko [53] used energy norm to measure the strength of transient growth. The energy norm is defined as

$$E_k = (\vec{q}, \vec{q})_2 = \int_0^\infty \vec{q}^T M \vec{q} dy \tag{20}$$

where the perturbation amplitude vector, $\vec{q}$, and the diagonal matrix, M, are expressed as

$$\vec{q} = (\hat{u}, \hat{v}, \hat{\rho}, \hat{T}, \hat{w})^T \tag{21}$$

$$M = diag[\rho, \rho, T/(\gamma \rho M e^2), \rho/(\gamma(\gamma-1)TMe^2), \rho] \tag{22}$$

In the current paper, the same energy norm is evaluated. The integral in Eq. (20) is numerical calculated across the boundary layer using a mid-point rule.

For receptivity simulations, boundary conditions of temperature and velocities on rough surface are linearly transferred to original smooth surface according to Eqs. (14) and (16). In order to evaluate the linear extrapolation, numerical simulations are carried out on different height surface roughness. Tables 1 and 2 list the heights of roughness elements with the spanwise wave number β being 0.3021 and 0.1511, respectively. Specifically, seven cases of numerical simulations on different height roughness are considered for $\beta = 0.3021$. Whereas four cases of numerical simulations on different height roughness are considered for $\beta = 0.1511$. In these two tables, the dimensional heights are non-dimensionalized by Blasius boundary-layer thickness at the center of roughness element, i.e., $x^* = 4.28125$ mm.

If linear boundary condition transfer is valid, the perturbation variables are linear to roughness height, and the energy norm in Eq. (20) is proportional to the square of roughness height. Figure 11 compares the energy norms for the seven cases of numerical simulations on different height roughness with the spanwise wave number being 0.3021. Furthermore, Fig. 12 compares the energy norms for the four cases of numerical simulations on different height roughness with the spanwise wave number being 0.1511. In each figure, the energy norm plotted by circular symbols is equal to the product of original norm for the case of "height $= 1 \times 10^{-6}$ m" and the square of roughness height ratio (> 1) between the two cases. For example, in Fig. 11(a), the ratio of roughness height between the two cases is three, the energy norm plotted by circular symbols is nine times of the original norm for the case of "height $= 1 \times 10^{-6}$ m". The good agreements between the two sets of energy norms in Figs. 11 (a) to 11 (d) indicate that the linear extrapolation of boundary condition is valid for roughness height up to 1×10^{-5}

m. Non-linear effect becomes important when surface roughness is higher than 1×10^{-5} m. The corresponding limitation of dimensionless roughness height for surface roughness is equal to 0.57850 as listed in Table 1. In Fig. 12 (a), the ratio of roughness height between the two cases is ten, the energy norm plotted by circular symbols is one hundred times of the original norm for the case of "height = 1×10^{-6} m". The agreement between the two sets of energy norms in Fig. 12 (a) indicates that the linear extrapolation of boundary condition is valid for roughness height of 1×10^{-5} m. In current study, the height of surface roughness is chosen to be 1×10^{-6} m, therefore the linear boundary condition transfer from rough surface to original smooth surface is valid.

To check the transient growth phenomena, one case of the receptivity of the hypersonic boundary layer to surface roughness is investigated. For this case, the parameters of surface roughness are as follows:

$$\epsilon = 1.0 \times 10^{-6}, \beta^* = 1.7355 \times 10^4 \mathrm{m}^{-1} \tag{23}$$

The dimensional wave number can be non-dimensionalized by Blasius boundary layer thickness at the center of the roughness element as:

$$\beta = \beta^* L^* = 0.3021 \tag{24}$$

Figure 13 plots the vector of $w\prime$ and $v\prime$ perturbations in the (y^*, z^*) plane at a location of $x^* = 5.4375$ mm ($R = 277.14$), 0.1875 mm downstream of the trailing edge of the roughness element. It is clearly shown that there is a pair of counter rotating streamwise vortices induced by surface roughness. With the streamwise vortices, momentum transfers from inviscid outer flow to the boundary layer, increasing the momentum in the boundary layer. Figure 14 shows energy norm distribution along the flat plate. It is noticed that the enery norm only has a small growth in the wake at the location of $x^* = 0.028$ m. The small energy norm increase may be caused by the small height of surface roughness. Figure 15 shows the distributions of streamwise and wall-normal velocity perturbations in wall-normal direction at the location of $x^* = 0.028$ mm. The strong oscillations of velocity perturbations outside the boundary layer ($40 < y^*/L^* < 100$) are related to the acoustic waves propagating along the Mach lines. Profiles of the two vecolity perturbations in the boundary layer indicate the exsitence of vorticity modes in the boundary layer, which is shown in Fig. 13.

To order to investigate the effect of spanwise wave number on transient growth, six cases of surface roughness with different spanwise wave numbers are considered. For all cases, the height of roughness is fixed to 1×10^{-6} m. Table 3 lists the spanwise wave numbers of surface roughness for the six cases, where the dimensional spanwise wave numbers are non-dimensionalized by Blasius boundary-layer thickness at the center of roughness element ($x^* = 4.28125$ mm). Figures 16 compares energy norm distributions along the flat plate near the roughness element for the six cases of surface roughness with different spanwise wave number. It shows the initial energy norm increases with the spanwise wave number increasing. In our simulations, surface roughness with even higher spanwise wave number has been tested. However they are not included in current paper, because the initial energy norm for even higher spanwise wave number is quite similar to that of $\beta = 0.0010$. Figure 17 compares energy norm distributions along the flat plate further downstream of the roughness element for the six cases of surface roughness with different spanwise wave number. It shows that the energy norm initially increases with the spanwise wave number increasing, however the energy norm of the case with $\beta = 0.0010$ is smaller than that of the case with $\beta = 0.0101$. Both Fig. 16 and Fig. 17 show that the spanwise wave number has a strong effect on transient growth. For the six cases considered in current study, surface roughness with the spanwise wave number being 0.0101 has the strongest excitation of transient growth.

5 Summary

The receptivity of a hypersonic flat-plate boundary layer to small surface roughness is investigated by series of numerical simulations. The free-stream flow conditions are the same as those of Maslov et al.'s leading-edge receptivity experiment [1]. Two-dimensional steady base flow is firstly achieved by solving compressible Navier-Stokes equations with a combination of a fifth-order shock-fitting method and a second-order TVD scheme. The accuracy of the numerical steady base flow is validated by comparisons with the theoretical self-similar boundary-layer solution and Maslov et al.'s experimental measurements. The three-dimensional base flow is directly extended from two-dimensional base flow due to the fact that the base flow over the flat plate is independent of spanwise coordinate. In receptivity simulations, small surface roughness, periodic in spanwise direction, is introduced on the flat plate. The subsequent responses of the hypersonic boundary layer are simulated by solving three-dimensional Navier-Stokes equations with a fifth-order shock-fitting method and a Fourier collocation method. Due to small

height of roughness element, boundary conditions of temperature and velocities on the rough surface are transferred to original smooth surface by linear extrapolation. The effect of spanwise wave number on the receptivity is studied by considering six cases of receptivity simulations. The numerical results show that counter rotating streamwise vortices and transient growth are induced by surface roughness. The spanwise wave number has a strong effect on the excitation of transient growth. For the six cases considered in current study, surface roughness with the spanwise wave number being 0.0101 has the strongest excitation of transient growth.

References

[1] A. A. Maslov, A. N. Shiplyuk, A. Sidorenko, and D. Arnal. Leading-edge receptivity of a hypersonic boundary layer on a flat plate. *Jounral of Fluid Mechanics*, Vol.426, pp.73-94, 2001.

[2] L. Lees and C. C. Lin. Investigation of the stability of the laminar boundary layer in compressible fluid. *NACA TN No. 1115*, 1946.

[3] L. M. Mack. Linear Stability Theory and the Problem of Supersonic Boundary-Layer Transition. *AIAA Journal*, Vol.13, No.3, pp.278-289, 1975.

[4] J. M. Kendall. Wind Tunnel Experiments Relating to Supersonic and Hypersonic Boundary-Layer Transition. *AIAA Journal*, Vol.13, No.3, pp.290–299, 1975.

[5] M. R. Malik, R. S. Lin, and R. Sengupta. Computation of Hypersonic Boundary-Layer Response to External Disturbances. *AIAA Paper 1999-0411*, January 1999.

[6] Y. Ma and X. Zhong. Receptivity of a supersonic boundary layer over a flat plate. Part 3. Effects of different types of free-stream disturbances. *Journal of Fluid Mechanics*, Vol.532, pp.63-109, 2005.

[7] E. Reshotko. Is Re_θ/Me a meaningful transition criterion ? *AIAA paper 2007-0943*, January 2007.

[8] M. V. Morkovin, E. Reshotko, and T. Herbert. Transition in open flow systems - a reassessment. *Bulletin of the American Physical Society*, Vol. 39, pp. 1882, 1994.

[9] W. S. Saric, H. L. Reed, and E. J. Kerschen. Boundary-layer receptivity to freestream disturbances. *Annual Review of Fluid Mechanics*, Vol. 34, pp. 291-319, 2002.

[10] M. E. Goldstein and L. S. Hultgren. Boundary-layer receptivity to long-wave free-stream disturbances. *Annual Review of Fluid Mechanics*, Vol.21, pp.137-166, 1989.

[11] A. V. Fedorov and A. P. Khokhlov. Receptivity of Hypersonic Boundary Layer to Wall Disturbances. *Theoretical and Computational Fluid Dynamics*, Vol.15, pp.231-254, 2002.

[12] A. Tumin, X. Wang, and X. Zhong. Direct numerical simulation and the theory of receptivity in a hypersonic boundary layer. *Physics of Fluids*, Vol. 19, Paper No. 014101, 2007.

[13] Y. Ma and X. Zhong. Receptivity of a supersonic boundary layer over a flat plate. Part 1:Wave Structures and Interactions. *Journal of Fluid Mechanics*, Vol.488, pp.31-78, 2003.

[14] Y. Ma and X. Zhong. Receptivity of a supersonic boundary layer over a flat plate. Part 2:Receptivity to Freestream Sound. *Journal of Fluid Mechanics*, Vol.488, pp.79-121, 2003.

[15] P. Balakumar, P. Hall, and M. R. Malik. On the receptivity and non-parallel stability of travelling disturbances in rotating disk flow. *ICASE Report*, No.90-89, 1990.

[16] F. P. Bertolotti. Vortex generation and wave-vortex interaction over a concave plate with roughness and suction. *ICASE Report*, No.93-101, 1993.

[17] M. Choudhari. Roughness-induced generation of crossflow vortices in three-dimensional boundary layers. *Theoretical and Computational Fluid Dynamics*, Vol.6, pp.1-30, 1994.

[18] A. Hanifi, P. J. Schmid, and D. S. Henningson. Transient growth in compressible boundary layer flow. *Physics of Fluids*, Vol.8, No.3, pp.826-837, 1996.

[19] P. Andersson, M. Berggren, and D. S. Henningson. Optimal Disturbances and Bypass Transition in Boundary Layers. *Physics of Fluids*, Vol.11, No.1, pp.134-150, 1999.

[20] T. Herbert. On the stability of 3D boundary layers. *AIAA paper 1997-1961*, June 1997.

[21] E. Reshotko. Transient growth: A factor in bypass transition. *Physics of Fluids*, Vol.13, No.5, pp.1067-1075, 2001.

[22] E. Forgoston and A. Tumin. Three-dimensional wave packet in a hypersonic boundary layer. *AIAA paper 2005-0099*, January 2005.

[23] A. A. Maslov and N. V. Semenov. Excitation of natural oscillations in a boundary layer by an external acoustic field. *Fluid Dynamics (Historical Archive)*, Vol.21, pp.400-404, 1986.

[24] M. Gaster, C. E. Grosch, and T. L. Jackson. The velocity field created by a shallow bump in a boundary layer. *Physics of Fluids*, Vol.6, No.9, pp.3079-3085, 1994.

[25] A. A. Bakchinov, G. R. Grek, B. G. B. Klingmann, and V. V. Kozlov. Transition experiments in boundary layer with embedded streamwise vortices. *Physics of Fluids*, Vol.7, No.4, pp.820-832, 1995.

[26] V. N. Vetlutskii, A. A. Maslov, S. G. Mironov, T. V. Poplavskaya, and A. N. Shiplyuk. Hypersonic flow on a flat plate. Experimental results and numerical modeling. *Journal of Applied Mechanics and Technical Physics*, Vol. 36, No. 6, pp. 848-854, 1995.

[27] E. B. White. Transient growth of stationary disturbances in a flat plate boundary layer. *Physics of Fluids*, Vol. 14, No. 12, pp. 4429-4439, 2002.

[28] E. B. White and F. G. Ergin. Receptivity and transient growth of roughness-induced disturbances. *AIAA paper 2003-4243*, June 2003.

[29] J. H. M. Fransson and L. Brandt. Experimental and theoretical investigation of the nonmodal growth of steady streaks in a flat plate boundary layer. *Physics of Fluids*, Vol. 16, No. 10, pp. 3627-3638, 2004.

[30] E. B. White, J. M. Rice, and F. G. Ergin. Receptivity of stationary transient disturbances to surface roughness. *Physics of Fluids*, Vol.17, No.6, Paper No.064109, 2005.

[31] T. Kawamura, H. Takami, and K. Kuwahara. Computation of high Reynolds number flow around a circular cylinder with surface roughness. *Fluid Dynamics Research*, Vol.1, pp.145-162, 1986.

[32] R. D. Joslin and C. E. Grosch. Growth characteristics downstream of a shallow bump: Computation and experiment. *Physics of Fluids*, Vol.7, No.12, pp.3042-3047, 1995.

[33] A. Bottaro and A. Zebib. Görtler vortices promoted by wall roughness. *Fluid Dynamics Research*, Vol.19, pp.343-362, 1997.

[34] C. Stemmer, M. J. Kloker, and S. Wagner. DNS of harmonic point source disturbances in an airfoil boundary layer flow. *AIAA paper 1998-2346*, June 1998.

[35] S. S. Collis and S. K. Lele. Receptivity to surface roughness near a swept leading edge. *Journal of Fluid Mechanics*, Vol.380, pp.141-168, 1999.

[36] X. Zhong. Leading-Edge Receptivity to Free Stream Disturbance Wave for Hypersonic Flow Over A Parabola. *Journal of Fluid Mechanics*, Vol.441, pp.315-367, 2001.

[37] H. Dong and X. Zhong. Numerical simulations of transient growth in a Mach 15 boundary layer over a blunt leading edge. *AIAA paper 2003-1266*, January 2003.

[38] I. V. Egorov, A. V. Fedorov, and V. G. Soudakov. Direct Numerical Simulation of Unstable Disturbances in Supersonic Boundary Layer. *AIAA paper 2004-0588*, January 2004.

[39] P. Fischer and M. Choudhari. Numerical simulation of roughness-induced transient growth in a laminar boundary layer. *AIAA paper 2004-2539*, June 2004.

[40] M. Choudhari and P. Fischer. Roughness-induced transient growth. *AIAA paper 2005-4765*, June 2005.

[41] Y. Ma and X. Zhong. Receptivity to Freestream Disturbances of Mach 8 Flow over A Sharp Wedge. *AIAA paper 2003-0788*, 2003.

[42] X. Wang and X. Zhong. Receptivity of A Mach 8.0 Flow over A Sharp Wedge to Wall Blowing-Suction. *AIAA paper 2005-5025*, June 2005.

[43] I. V. Egorov, V. G. Sudakov, and A. V. Fedorov. Numerical modeling of the stabilization of a supersonic flat-plate boundary layer by a porous coating. *Fluid Dynamics*, Vol. 41, No. 3, pp. 356-365, 2006.

[44] X. Zhong and Y. Ma. Boundary-layer receptivity of Mach 7.99 flow over a blunt cone to free-stream acoustic waves. *Journal of Fluid Mechanics*, Vol.556, pp.55-103, 2006.

[45] X. Zhong. High-Order Finite-Difference Schemes for Numerical Simulation of Hypersonic Boundary-Layer Transition. *Journal of Computational Physics*, Vol.144, pp. 662-709, 1998.

[46] X. Zhong. Additive Semi-Implicit Runge-Kutta Schemes for Computing High-Speed Nonequilibrium Reactive Flows. *Journal of Computational Physics*, Vol.128, pp.19-31, 1996.

[47] X. Zhong and T. Lee. Nonequilibrium real-gas effects on disturbance/bow shock interaction in hypersonic flow past a cylinder. *AIAA paper 1996-1856*, January 1996.

[48] A. Tumin, X. Wang, and X. Zhong. Direct Numerical Simulation of Receptivity in a Hypersonic Boundary Layer: Validation. *AIAA paper 2006-1108*, January 2006.

[49] X. Zhong. Receptivity of Mach 6 flow over a flared cone to freestream disturbance. *AIAA paper 2004-0253*, January 2004.

[50] X. Wang and X. Zhong. Numerical simulation of hypersonic boundary-layer receptivity to two and three-dimensional wall perturbations. *AIAA paper 2007-0946*, January 2007.

[51] Y. Ma and X. Zhong. Receptivity to Freestream Disturbances of Mach 4.5 Flow over A Flat Plate. *AIAA Paper 2002-0140*, January 2002.

[52] X. Wang and X. Zhong. Numerical Simulation and Experiment Comparison of Leading-Edge Receptivity of A Mach 5.92 Boundary Layer. *AIAA paper 2006-1107*, January 2006.

[53] A. Tumin and E. Reshotko. Spatial Theory of Optimal Disturbances in Boundary Layers. *Physics of Fluids*, Vol.13, No.7, 2001.

n	ϵ	Dimensional height (m)	Dimensionless height
1	1.0×10^{-6}	1.0×10^{-6}	0.05785
2	3.0×10^{-6}	3.0×10^{-6}	0.17355
3	5.0×10^{-6}	5.0×10^{-6}	0.28925
4	8.0×10^{-6}	8.0×10^{-6}	0.46280
5	1.0×10^{-5}	1.0×10^{-5}	0.57850
6	5.0×10^{-5}	5.0×10^{-5}	2.89251
7	1.0×10^{-4}	1.0×10^{-4}	5.78502

Table 1: Heights of surface roughness with the spanwise wave number being 0.3021 for the seven cases of numerical simulations.

n	ϵ	Dimensional height (m)	Dimensionless height
1	1.0×10^{-6}	1.0×10^{-6}	0.05785
2	1.0×10^{-5}	1.0×10^{-5}	0.57850
3	5.0×10^{-5}	5.0×10^{-5}	2.89251
4	1.0×10^{-4}	1.0×10^{-4}	5.78502

Table 2: Heights of surface roughness with the spanwise wave number being 0.1511 for the four cases of numerical simulations.

n	Dimensional spanwise wave number (m^{-1})	Dimensionless spanwise wave number
1	1.73550×10^4	0.3021
2	8.67752×10^3	0.1511
3	5.78502×10^3	0.1007
4	2.89251×10^3	0.0504
5	5.78502×10^2	0.0101
6	57.85016	0.0010

Table 3: The spanwise wave numbers of surface roughness for the six cases of receptivity simulations.

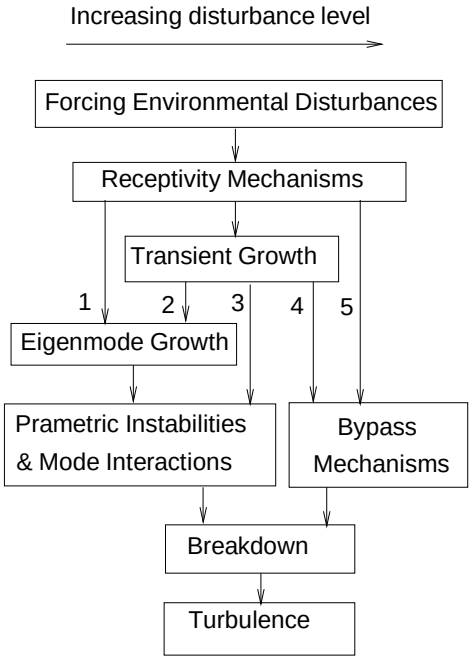

Figure 1: Paths of boundary-layer transition process respecting to disturbance amplitude.

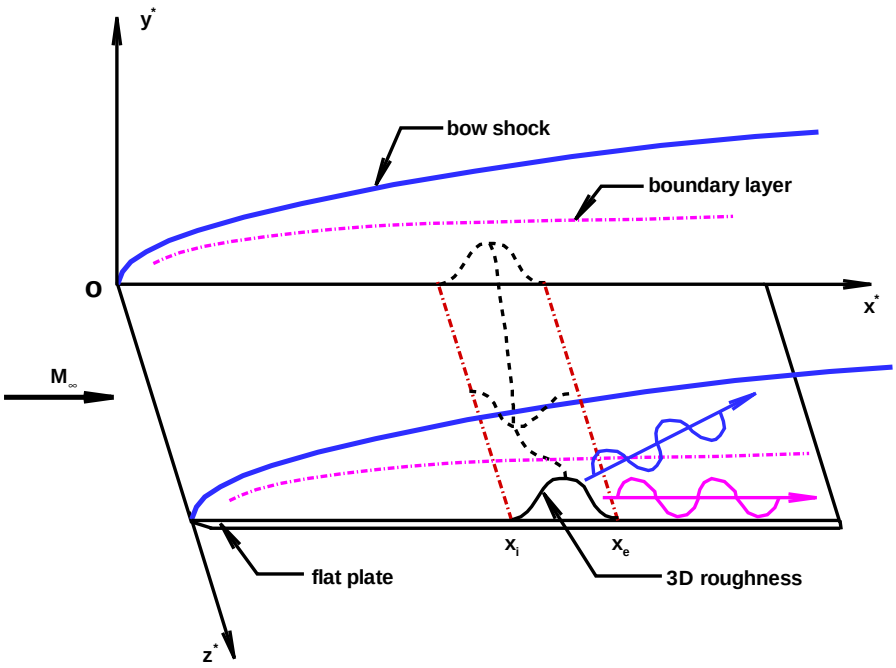

Figure 2: A schematic of the receptivity of the Mach 5.92 flow to three-dimensional surface roughness.

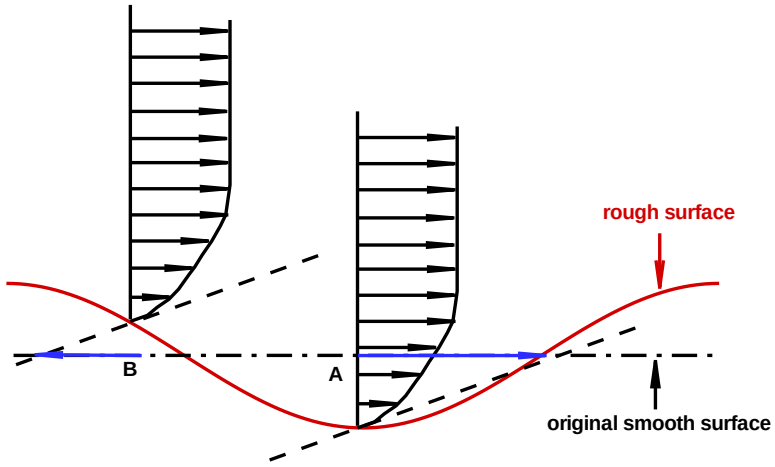

Figure 3: A schematic of linear boundary condition transfer of streamwise velocity for points A and B on original smooth surface.

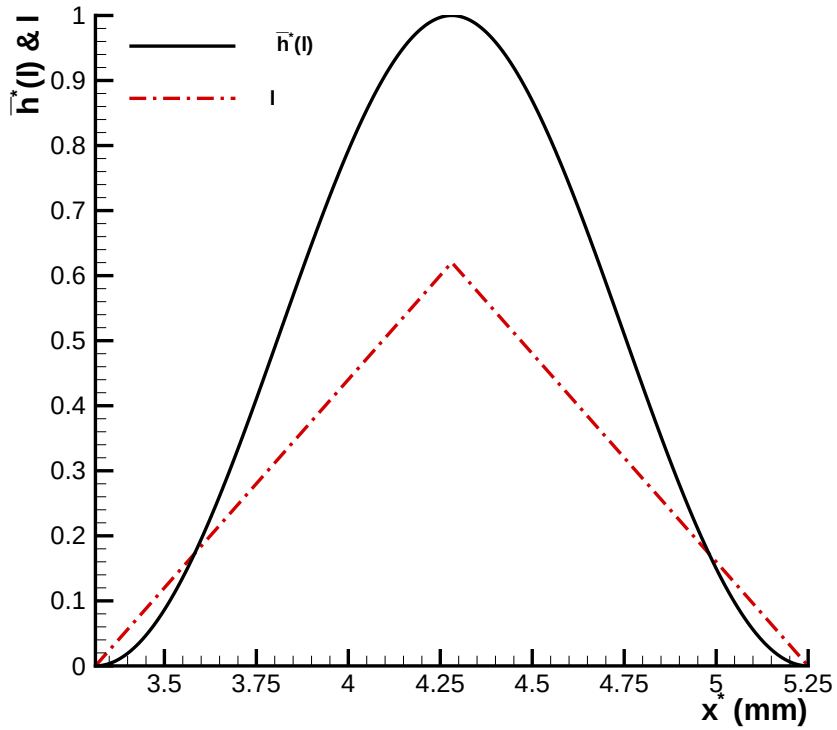

Figure 4: The profile function $\hbar^*(l)$ and the variable l of the roughness element in streamwise direction.

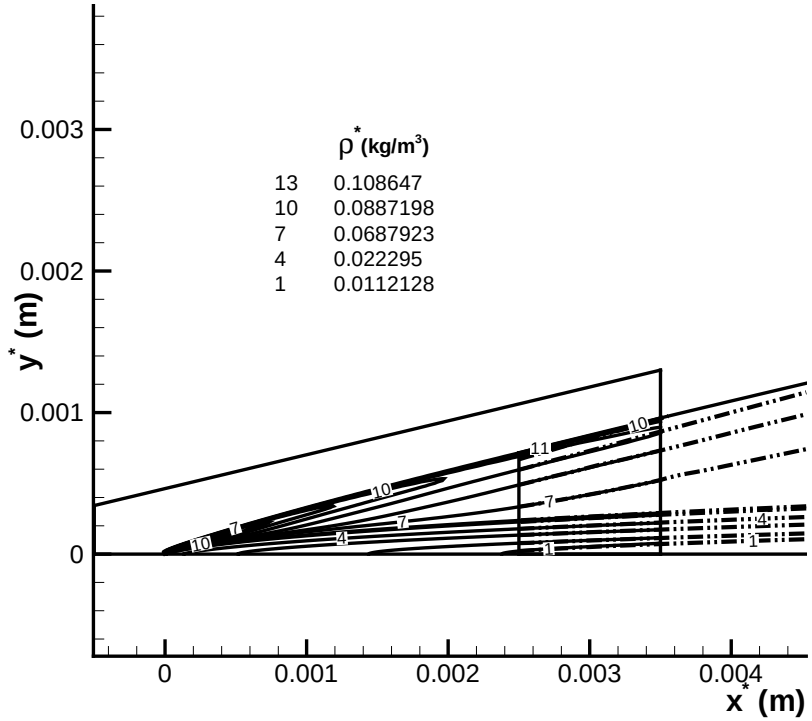

Figure 5: Density contours near the leading edge of the base flow obtained by the combination of second-order TVD scheme and fifth-order shock-fitting method.

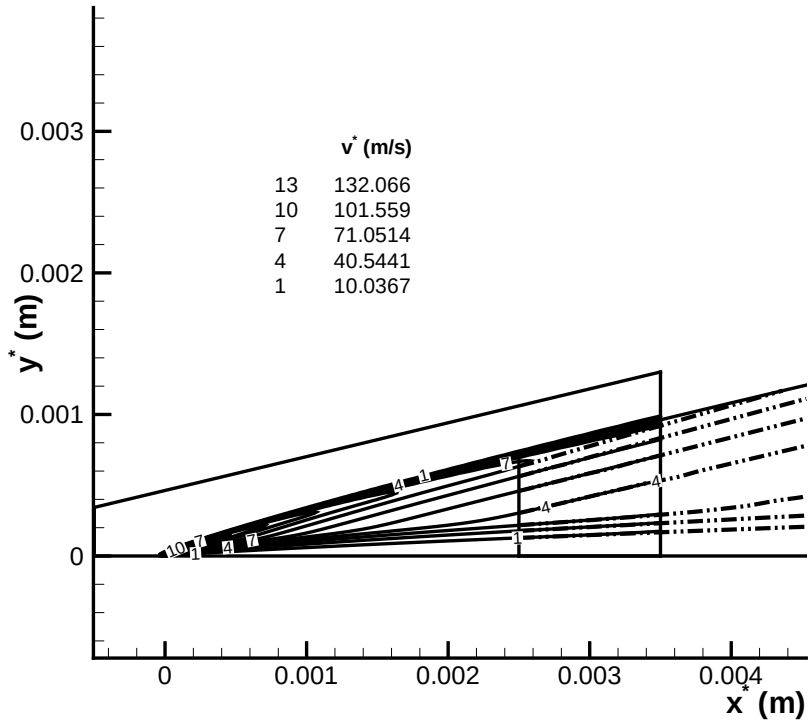

Figure 6: Wall-normal velocity contours near the leading edge of the base flow obtained by the combination of second-order TVD scheme and fifth-order shock-fitting method.

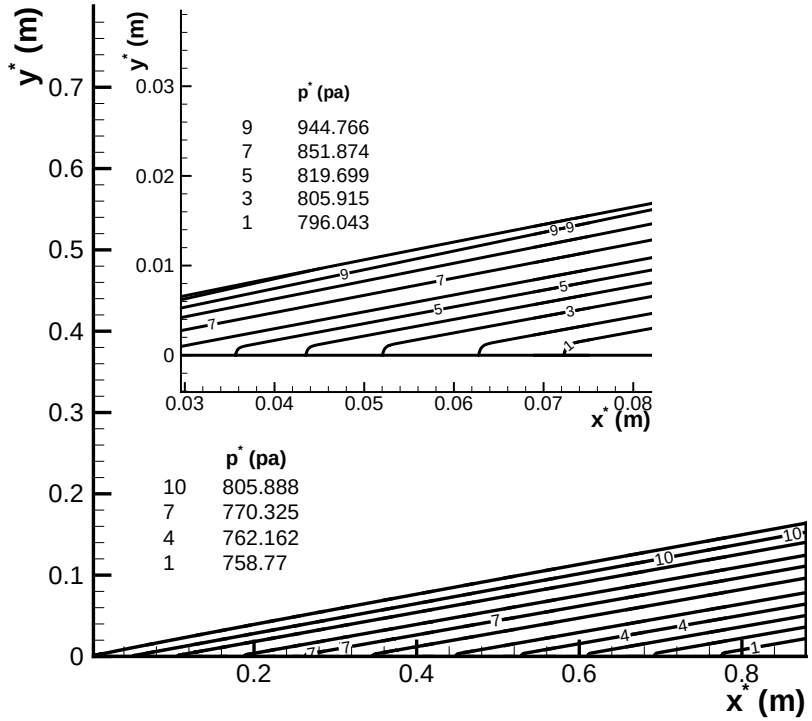

Figure 7: Pressure contours of the base flow simulated by the fifth-order shock-fitting method.

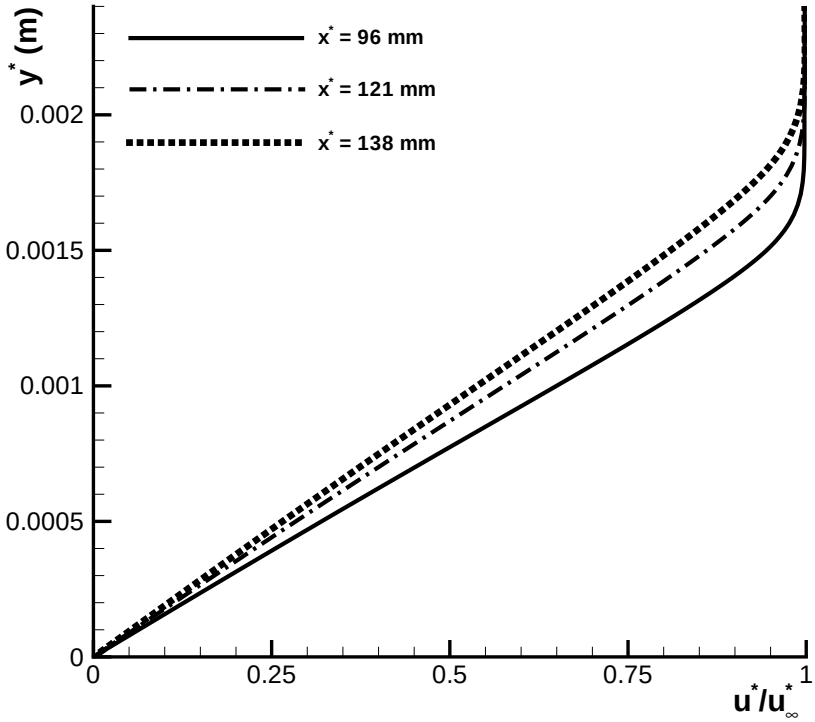

Figure 8: Distributions of dimensionless streamwise velocity across the boundary layer of the numerical base flow at three different locations.

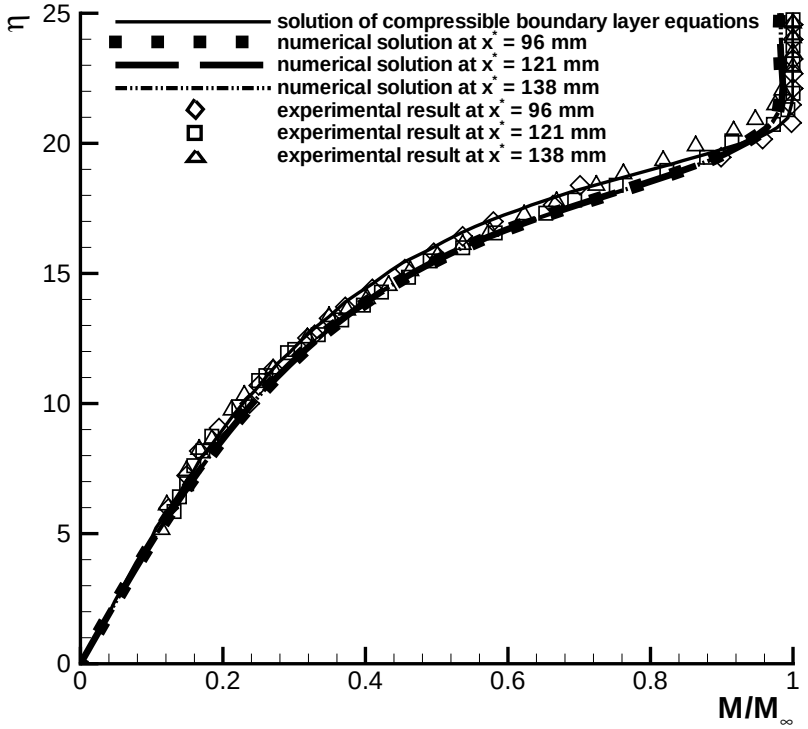

Figure 9: Comparison of normalized Mach number distributions across the boundary layer at three different locations.

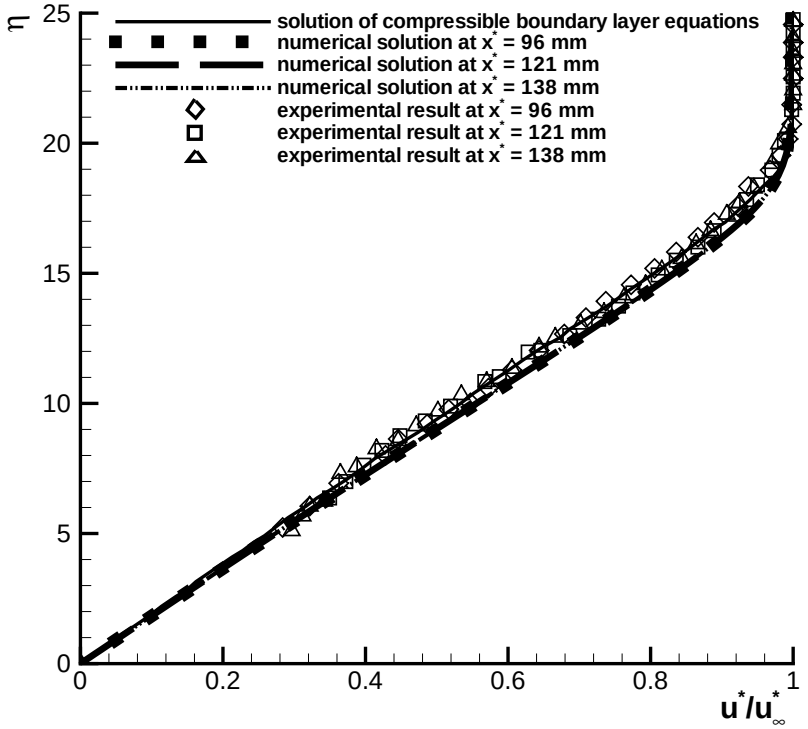

Figure 10: Comparison of dimensionless streamwise velocity distributions across the boundary layer at three different locations.

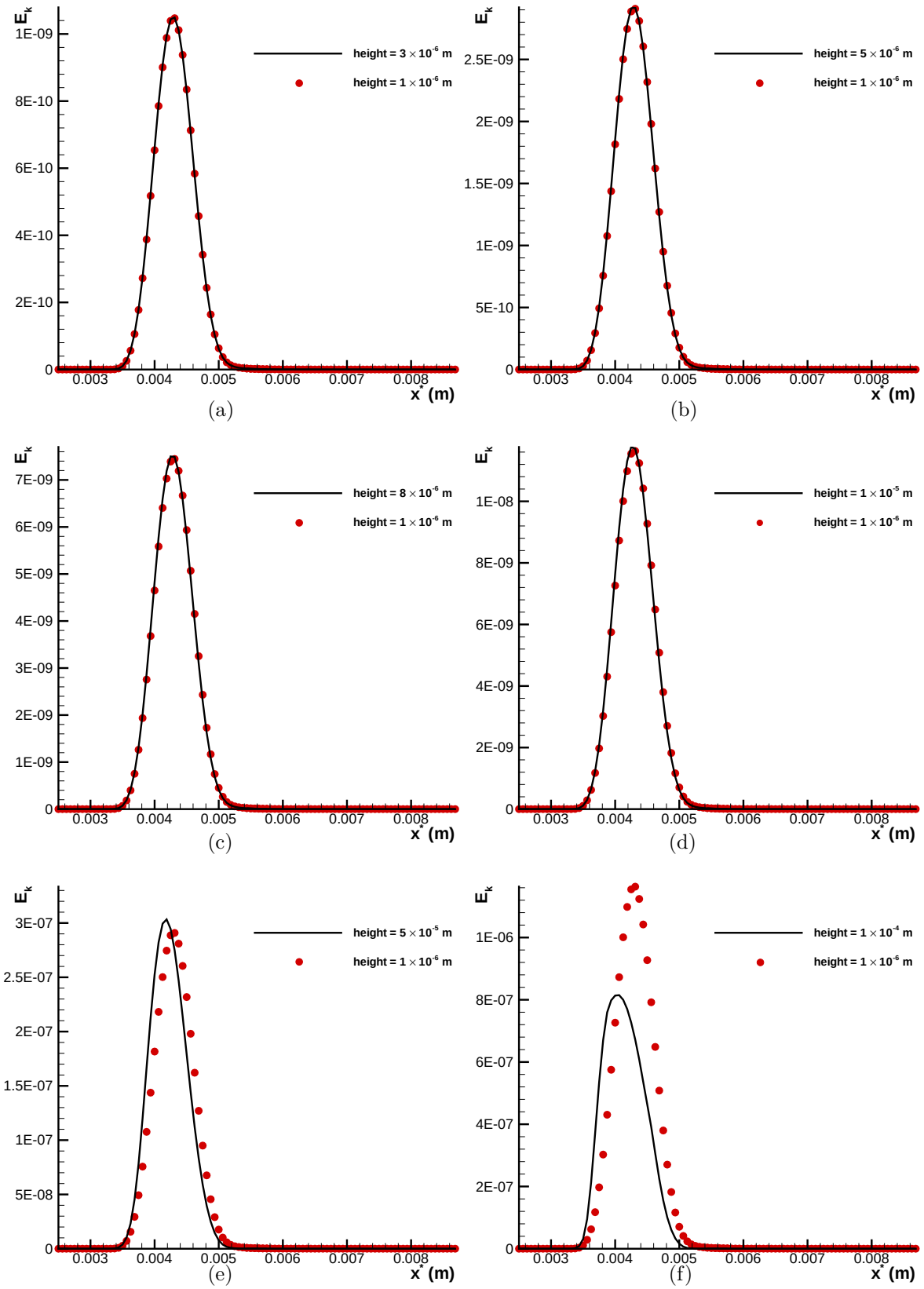

Figure 11: Energy norm comparisons for the seven cases of numerical simulations on different height roughness with the spanwise wave number being 0.3021.

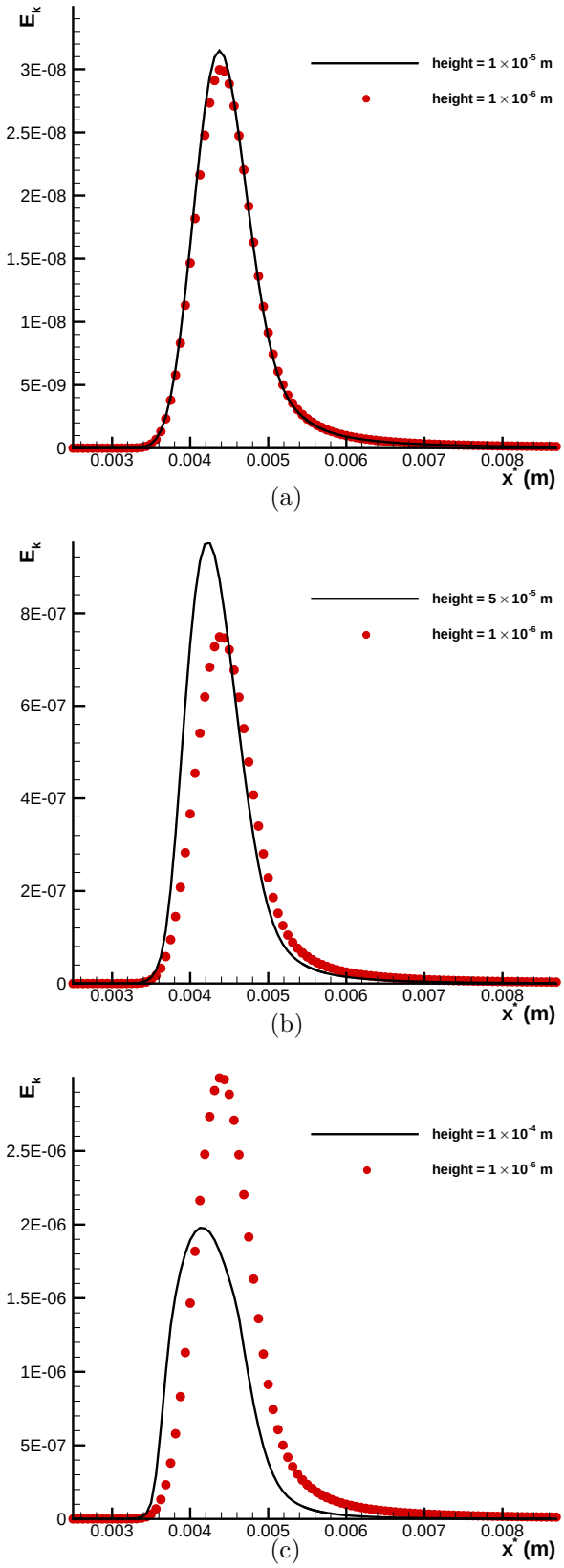

Figure 12: Energy norm comparisons for the four cases of numerical simulations on different height roughness with the spanwise wave number being 0.1511.

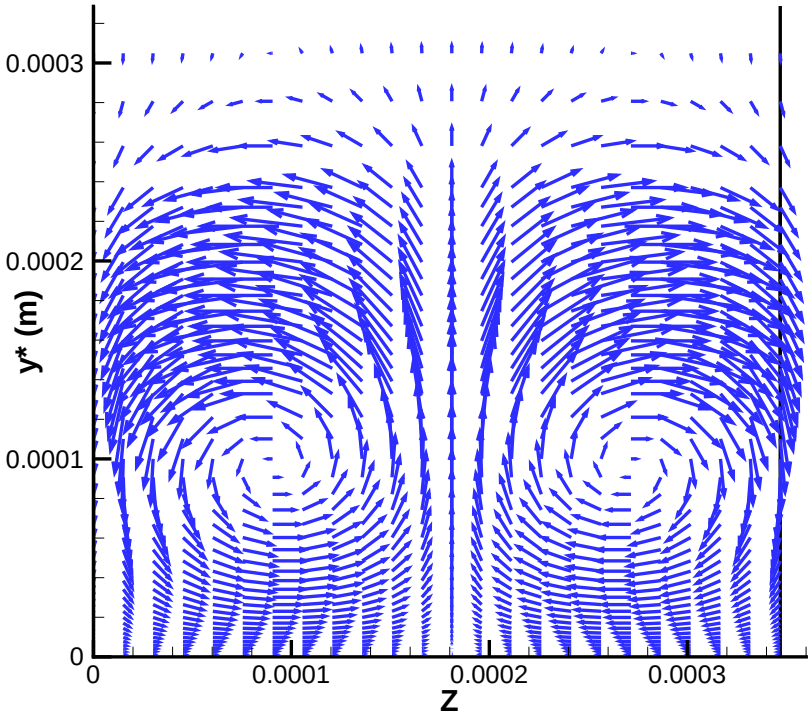

Figure 13: Vector plot of $w\prime$ and $v\prime$ perturbations in the (y^*, z^*) plane at the location of $x^* = 5.4375$ mm for the case of surface roughness with $\beta = 0.3021$.

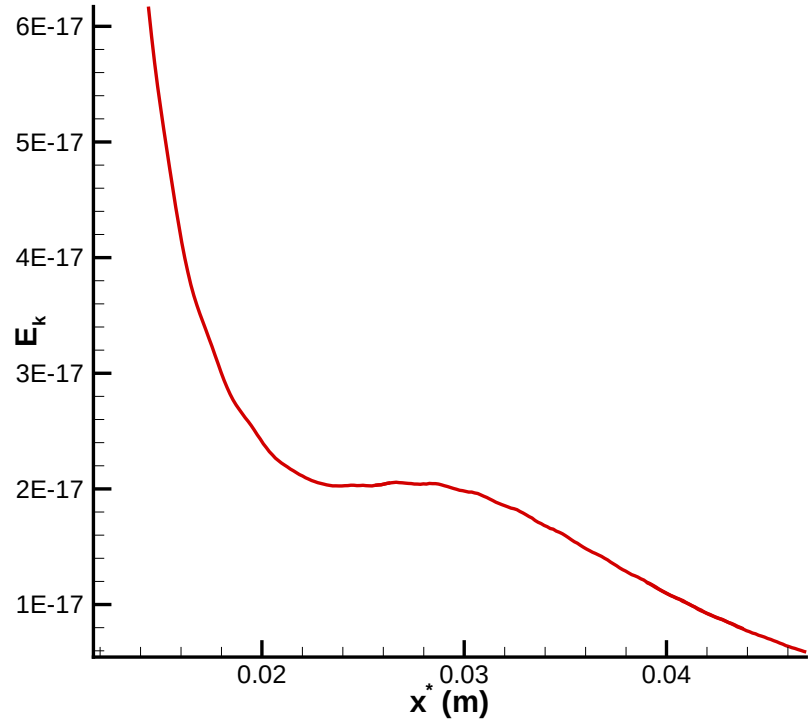

Figure 14: Energy norm distribution along the flat plate for the case of surface roughness with $\beta = 0.3021$.

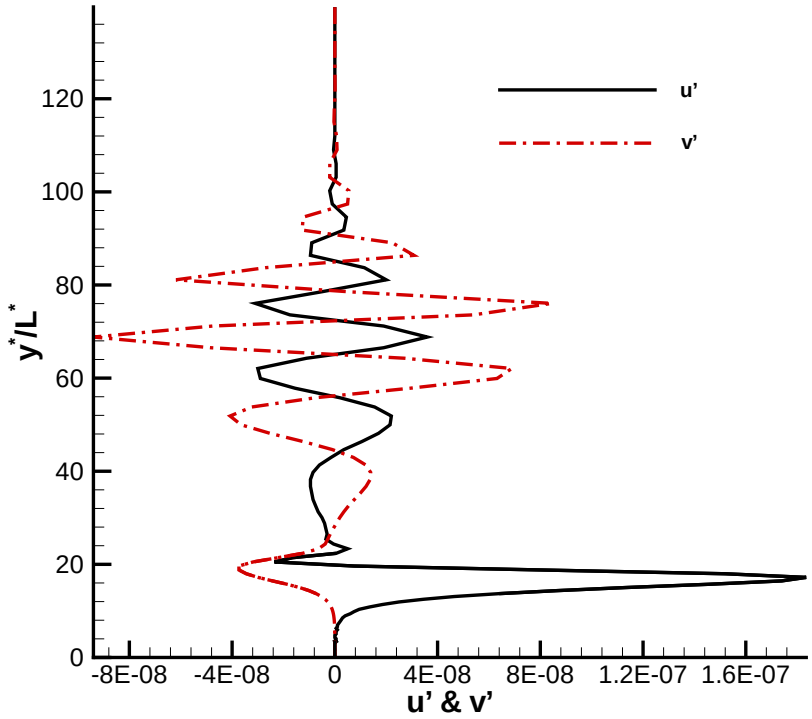

Figure 15: Streamwise and wall-normal velocity perturbations in wall-normal direction at the location of $x^* = 0.028$ m.

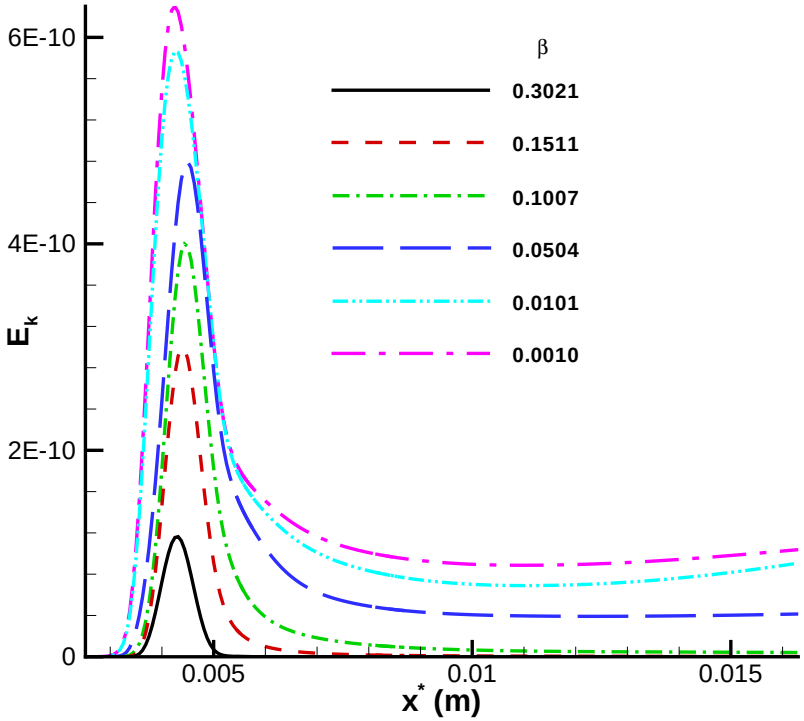

Figure 16: Energy norm distributions along the flat plate near the roughness element for the six cases of surface roughness with different spanwise wave number.

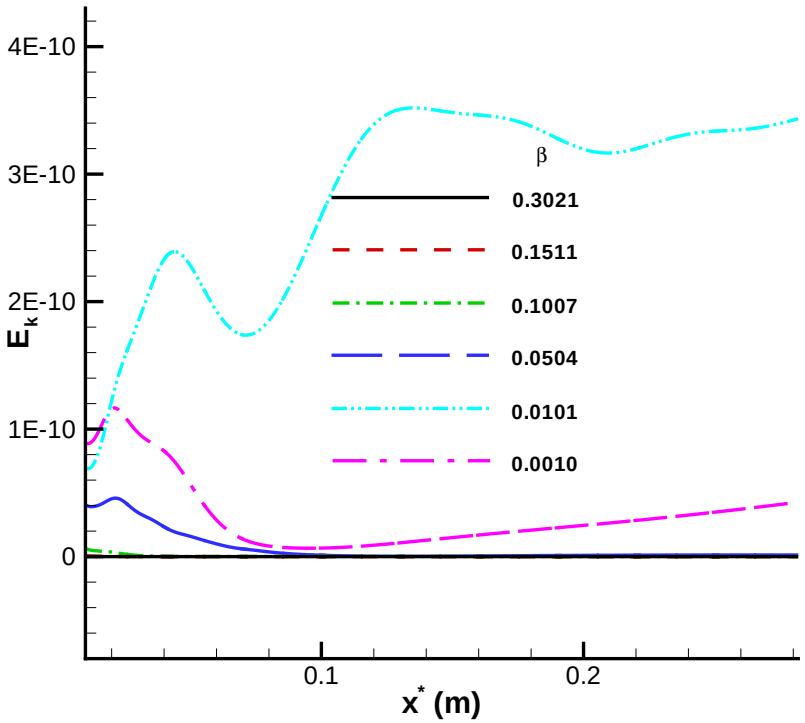

Figure 17: Energy norm distributions along the flat plate further downstream of the roughness element for the six cases of surface roughness with different spanwise wave number.